Title

Atomic Orbital Alignment and Coherence in N2O Photodissociation at 193.3 nm

Authors

Ahmed, Musahid
Wouters, Eloy R
Peterka, Darcy S
et al.

Publication Date

1999-03-01

LBNL-43097
Preprint

ERNEST ORLANDO LAWRENCE
BERKELEY NATIONAL LABORATORY

Atomic Orbital Alignment and Coherence in N_2O Photodissociation at 193.3 nm

Musahid Ahmed, Eloy R. Wouters, Darcy S. Peterka,
Oleg S. Vasyutinskii, and Arthur G. Suits

Chemical Sciences Division

March 1999

Submitted to
Faraday Discussion #113

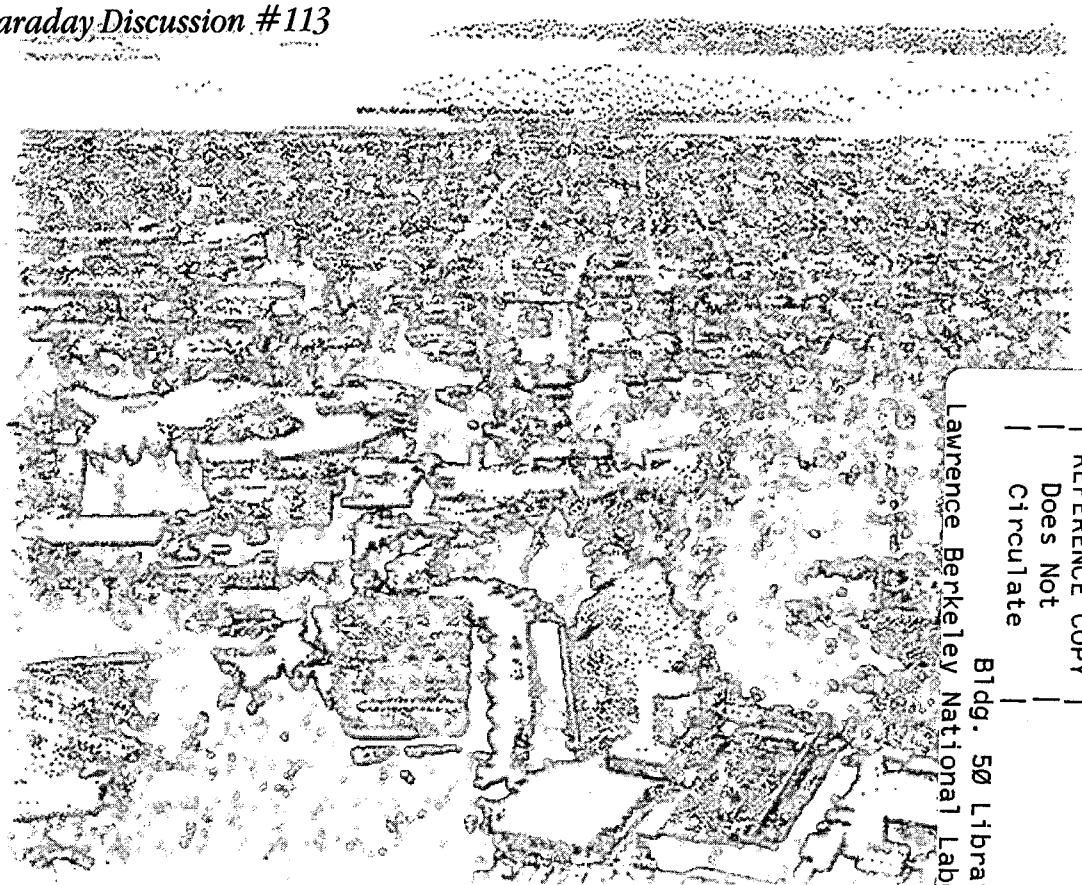

DISCLAIMER

LBNL-43097

Atomic Orbital Alignment and Coherence in N_2O Photodissociation at 193.3 nm

Musahid Ahmed,[a] Eloy R. Wouters,[a] Darcy S. Peterka,[a]
Oleg S. Vasyutinskii,[b] and Arthur G. Suits[a]

[a]Chemical Sciences Division
Ernest Orlando Lawrence Berkeley National Laboratory
University of California
Berkeley, California 94720

[b]Ioffe Institute
Russian Academy of Sciences
194021 St. Petersburg, Russia

March 1999

This work was supported by the Director, Office of Science, Office of Basic Energy Sciences, Chemical Sciences Division, of the U.S. Department of Energy under Contract No. DE-AC03-76SF00098.

Corresponding Author:

Arthur G. Suits
Chemical Sciences Division MS 6-2100
Ernest Orlando Lawrence
Berkeley National Laboratory
1 Cyclotron Road
Berkeley CA 94720

Atomic Orbital Alignment and Coherence in N_2O Photodissociation at 193.3 nm

Musahid Ahmed,[a] Eloy R. Wouters,[a] Darcy S. Peterka,[a]

Oleg S. Vasyutinskii[b] and Arthur G. Suits[a,*]

[a] *Chemical Sciences Division,*

Ernest Orlando Lawrence Berkeley National Laboratory, Berkeley, CA 94720, USA

[b] *Ioffe Institute, Russian Academy of Sciences, 194021 St. Petersburg, Russia*

Strong recoil-frame orbital alignment is observed in the $O(^1D_2)$ product following photodissociation of N_2O at 193.3 nm. Velocity map imaging allows for investigation of the angular distribution of this alignment, providing insight into the dynamics in the frame of the molecule. Analysis of the results using a rigorous quantum mechanical theory yields alignment anisotropy parameters having direct physical significance. This alignment is dominated by strong incoherent parallel and perpendicular contributions. In addition, evidence is shown of a contribution from a perpendicular coherence. These results provide detailed insight into the dynamics of the photodissociation process and the nature of the electronic transitions responsible for the initial excitation.

I Introduction

In a widely cited 1987 review,[1] J. P. Simons eloquently summarized the conceptual motivation for studying the correlations among vector quantities in reaction dynamics: '... the measurement of correlations involving axial or angular momentum vectors provides an entry into the anisotropy of molecular interactions, an approach to understanding the stereospecificity of chemical reactivity, and a means of charting the collision dynamics in stereoscopic 3-D.' Since the 1980s, experimentalists have been very successful at probing vector correlations in photodissociation.[2] Initial studies[3]

probed the correlation of the fragments' recoil velocity vector **v** with the laser polarization direction **e**, i.e., the photofragment angular distribution or velocity anisotropy, characterized by the familiar anisotropy parameter β. Another important vector correlation in photochemical studies is that between the **e** vector and the projection of the angular momentum **J** of the photofragments on the space-fixed Z-axis.[4] These are characterized by the moments of the magnetic sublevel distribution: the population, which is independent of the magnetic sublevel m distribution, the orientation, which is proportional to the dipole moment of the ensemble and implies a nonstatistical m distribution, or the alignment, which is proportional to the quadrupole moment of the ensemble and implies a nonstatistical $|m|$ distribution.[5] These measurements can provide important information about the dissociation dynamics, the shape of the potential curves, the symmetries of excited states and the role of nonadiabatic interactions. Another important aspect of vector correlations in photodissociation studies is the correlation between the photofragment recoil direction **v**, and the photofragment angular momentum **J**, or the *angular distribution* of the angular momentum polarization.[6] This has been studied in considerable detail for photofragment rotational angular momentum, where the experiments can sometimes provide insight into the broad features of the dissociation dynamics and the nature of the transition state.

Owing in part to several experimental innovations, a number of groups recently have begun investigations of this same **v**–**J** correlation for photofragment atomic orbital polarization, using either the ion imaging technique,[7] in which these effects can be dramatically evident, or Doppler[8] or ion time-of-flight profiles.[9] These studies have the potential to provide insight into the underlying photophysics in the frame of the molecule. Much of the recent work has relied on an analysis in which coherences, i.e., the off-diagonal elements of the density matrix, are assumed to vanish and only the diagonal elements of the density matrix, the magnetic sublevel populations, are inferred. However, recent work in our laboratory,[10] and in the Zare laboratory,[11] building on a theoretical foundation provided by Siebbeles and coworkers[12] and Vasyutinskii and coworkers, [13] has shown that these coherence effects are by no means negligible, and in fact may be used to provide new insights into the photodissociation dynamics. We have applied these methods to the study the photochemistry of Cl_2 and NO_2, and here extend them to the analysis of the alignment of the $O(^1D_2)$ product of N_2O photolysis at 193.3 nm.

Photodissociation of N_2O in the deep ultraviolet has been the subject of a number of studies owing to its importance in the atmosphere and its use as a precursor for $O(^1D_2)$ production for reactive scattering experiments. In some of these scattering studies,[14] with state-resolved product detection conducted under bulb rather than crossed-beam conditions, the overall 'velocity anisotropy' or photofragment angular distribution, as well as the details of the orbital polarization, may be very important for a detailed understanding and interpretation of the results of the reactive scattering experiments. We have undertaken the present study of N_2O photodissociation in an effort to enrich the understanding of the fundamental photodissociation dynamics of N_2O, and to provide a firm foundation for the interpretation of the scattering studies relying on N_2O to produce $O(^1D_2)$. This study relies on our recently developed techniques providing a rigorous connection between ion imaging measurements and alignment anisotropy parameters having explicit physical significance.

N_2O photodissociation has been studied at a number of wavelengths in the vicinity of 200 nm. The ArF excimer line at 193.3 nm occurs near the onset of UV absorption in N_2O, so several groups have examined its photodissociation dynamics there. Felder and Huber[15] used photofragment translational spectroscopy (PTS) with a universal detector to record the translational energy distributions [$P(E)$] and photofragment angular distributions. They found a $P(E)$ sharply peaked at 26 kcal/mol and an anisotropy parameter of 0.48. Houston and coworkers recorded Doppler profiles of the $O(^1D_2)$ from 193 nm photolysis of N_2O using 1-photon laser induced fluorescence (LIF) in the vacuum ultraviolet, with results that agreed quite well with the PTS measurements. In addition to the excimer-based studies, both of the dominant products, $O(^1D_2)$ and N_2, possess convenient transitions for 2+1 resonant ionization in the vicinity of 200–205 nm. As a result, a number of '1-laser' experiments (in which the same color is used to photolyse and probe) have been performed in this wavelength region. Shafer and coworkers recorded Doppler profiles of the $O(^1D_2)$ in a one-laser experiment at 205 nm. They obtained a limiting value of 2 for the anisotropy parameter, but their results preceded the PTS measurement, so, unlike Houston and coworkers, they were unable to use the guidance of the PTS $P(E)$ measurement to disentangle the translational energy and angular distributions. Hansico and Kummel studied the detailed N_2 rotational populations in 1-laser experiments at 203–207 nm, and found distributions peaking at J=73, with an inferred translational energy distribution agreeing reasonably well with Felder and with Houston. More recently, Suzuki et al. reported a 1-laser imaging study at 205 nm in which evidence of orbital alignment was presented and a bimodal translational energy distribution was inferred.[7b] Finally, Chandler and coworkers have reported both the alignment of the $O(^1D_2)$ at 205 nm[19] and very detailed measurements of the J-dependence of the anisotropy in the N_2, again in 1-laser experiments in the range 200–205 nm. Despite the abundance of studies in this wavelength region, a consensus on the detailed dissociation dynamics and alignment has yet to emerge, and no one to date has considered the role of coherences in the $O(^1D_2)$ product.

II Experimental

The molecular beam apparatus, described in detail in a recent publication,[21] consists of a skimmed molecular beam crossed by counterpropagating 30 Hz photolysis and probe lasers on the axis of a velocity map imaging time-of-flight mass spectrometer as shown schematically in Fig. 1. The molecular beam was produced by expanding pure N_2O from a piezoelectric pulsed valve. The photolysis laser was an ArF excimer, attenuated to 10 mJ/pulse, focused by an f = 30 cm lens into the interaction region. The $O(^1D_2)$ product was probed on a 2+1 REMPI transition[22] ($^1F_3 \leftarrow\leftarrow {}^1D_2$ at 203.8 nm, or $^1P_1 \leftarrow\leftarrow {}^1D_2$ at 205.4 nm) which was scanned over during image acquisition to encompass the full Doppler spread of the oxygen atom product. Each image is an average of at least 32,000 laser shots. Some contribution from background ions originating from the photolysis laser alone were subtracted from the data images shown, but note that our analysis method is self-correcting when isolating the alignment contribution (see below). In addition, the contribution to the signal from the probe laser alone was subtracted from the data images. The probe light was produced by doubling the output of an Nd-YAG pumped dye laser in β-barium borate (BBO), then mixing the resulting doubled light with the visible in a second BBO crystal, after adjusting the polarizations using a waveplate.

The probe light was focused into the interaction region using an f = 30 cm lens. Polarization of the photolysis laser was accomplished using a series of ten quartz plates fixed at Brewster's angle, yielding a 90% polarized beam. Rotation of the polarization of both lasers was accomplished using half-wave plates (Karl Lambrecht). The resulting O^+ ions were accelerated under momentum-focusing ('velocity mapping') conditions[23] toward a 80 mm diameter dual microchannel plate (MCP) coupled to a phosphor screen and imaged on a fast scan charge-coupled device camera with integrating video recorder (Data Design AC-101M). Two dissociation geometries were employed: the photolysis laser polarization was parallel (geometry I) or perpendicular (geometry II) to the ion time-of-flight axis, and the probe laser polarization was then fixed either parallel or perpendicular to the photolysis polarization to probe the atomic alignment.

III Results and Analysis

For the $O(^1D_2)$ product, state multipoles up to rank $K \leq 2j = 4$ are necessary for a complete description of the orbital polarization. In this report, however, we confine ourselves to a detailed analysis of the dominant rank 0 and 2 contributions. The odd multipoles may be present but are not probed when only linear polarizations are used. To further decrease the significance of rank 4 alignment terms, we have chosen to probe the $O(^1D_2)$ alignment via the $^1F_3$ intermediate state. For this particular probe transition, the detection efficiency for quadrupole components to the alignment, as expressed in the linestrength factor ratio P_4 / P_0 can be easily calculated[7a, 24] to be –0.11, and is the lowest of all three possible probe transitions. For the $^1P_1 \leftarrow\leftarrow {}^1D_2$ transition at 205.4 nm, $P_4 / P_0 = -1.1$. This line is thus particularly sensitive to the rank 4 contribution. Note that for the third possible probe transition $^1D_2 \leftarrow\leftarrow {}^1D_2$ at 198.5 nm, $\Delta J = \Delta L = 0$, and the evaluation of the linestrength factors becomes more complicated.

Measurement of the total laboratory frame alignment is important to scale the image data accurately.[10b] We obtain a value of $I_{par} / I_{perp} = 0.88 \pm 0.14$, where I_{par} refers to parallel polarizations of photolysis and probe lasers, and I_{perp} refers to perpendicular photolysis and probe laser polarizations. For the $O(^1D_2)$ atom there is no net nuclear or electron spin, so that there is no corresponding depolarization of the alignment on the timescale of the probe. Using the expression:[10b]

$$\frac{I_{par} - I_{perp}}{I_{par} + 2I_{perp}} = \frac{V(j)}{2\sqrt{5}} \frac{P_2}{P_0} \langle A_{20} \rangle ,$$

with the ratio of linestrength factors $P_2 / P_0 = 0.68$ and $V(j) = 5\sqrt{2/7}$, we obtain for the total alignment $\langle A_{20} \rangle$ –0.11. This value for $\langle A_{20} \rangle$ represents a relatively small laboratory frame alignment. Nevertheless, the imaging technique allows us to identify a large recoil-frame alignment, as shown below, despite the fact that the angle-averaged alignment is small.

The data images are shown in Fig. 2 for the indicated combination of photolysis and probe polarizations. Subtraction of the two images for different probe polarizations allows us to isolate the pure alignment signal from the dominant number-density

contribution.[10a,b] These difference images are shown in the third row of Fig. 2 for each photolysis polarization geometry. The alignment images were analyzed using two alternative techniques based upon basis images showing the different contributions to the alignment angular distributions. These contributions are characterized by four alignment anisotropy parameters,[13] s_2, α_2, η_2, and γ_2. The first two describe incoherent parallel and perpendicular contributions: s_2 represents the "intrinsic" portion of the incoherent contribution that vanishes after averaging over all recoil angles, while α_2 exhibits a characteristic angular dependence. The remaining parameters characterize the coherent contributions to the alignment: η_2 embodies the coherences among perpendicular components and γ_2 coherences between perpendicular and parallel contributions.

A first step to analyzing the data involves extracting the recoil speed and energy distributions [$P(v)$ and $P(E)$] using the inverse Abel transform. This is applicable to the geometry in which both lasers are parallel to the detector plane, since cylindrical symmetry is preserved in that case. In theory, the presence of the alignment can distort the measured $P(E)$ if there is strong coupling between the angular and translational energy distributions. That is, if there were both an angular dependence to the recoil velocity distribution and an angular dependence to the detection efficiency, then the reconstructed distribution would be in error. However as the net alignment is small, (since it is dominated by the s_2 contribution), the use of the inverse Abel transform to reconstruct the $P(E)$ should not lead to inaccuracies. The resulting $P(E)$ is shown in Fig. 3, and agrees reasonably well with the results of Huber et al.,[15] and Houston and coworkers.[16]

One approach to the analysis of the photofragment orbital alignment involves a fit of the entire difference image to a linear combination of basis images produced using expressions reported elsewhere,[10b] by means of the singular value decomposition (SVD) technique. In the underlying case of N_2O, the velocity distribution is not as sharply peaked as in our previous study of Cl_2 photodissociation. This effectively smears out the difference images, just as the finite experimental resolution does. To account for these effects in a first order approximation, we have convoluted the basis images with a Gaussian distribution to match the experimental images. The difference images are then fitted using the SVD technique, which yields the simulated images, shown along with the experimental difference images in Fig. 2 (bottom row). The values for the alignment parameters extracted from the analysis are summarized in Table I. These show the predominance of the s_2 component indicating both incoherent parallel and perpendicular contributions. However, in addition to the incoherent contribution, a significant value is obtained for the η_2 parameter, indicating a coherent perpendicular contribution to the alignment angular distribution.

A second approach involves fitting the angular behavior of the outer ring of the difference distribution, using basis curves obtained from the same basis images. This method was employed in the analysis of the NO_2 results,[10c] which were complicated by a bimodal recoil velocity distribution, making the calculation of basis images used in the SVD approach more difficult. The resulting simulated curves are shown in Fig. 4 along with the analogous curves derived from the alignment images, and a similar plot in which the coherent contributions were forced to vanish. The results, shown in Table I, agree well with the SVD based fit, showing the large negative s_2 value and a significant value for η_2. The nonzero γ_2 parameter is likely not significant, as indicated by the large error

bar for that parameter and the much smaller error bars for the corresponding value from the SVD approach.

The remaining quantity of interest is the photofragment angular distribution, characterized by the familiar β parameter. For an image without alignment effects, for instance in the case that P_2 and P_4 linestrength factors are zero, the anisotropy parameter can be found by simply fitting the usual expression $I(\theta) \propto 1 + \beta P_2(\cos\theta)$ (with $P_2(\cos\theta)$ the second order Legendre polynomial in $\cos\theta$, where θ is the angle with respect to the photolysis laser polarization) to the inverse Abel transformed image with both laser polarization parallel to the detector (M_Y in geometry II). Unfortunately, alignment effects distort this picture. As was mentioned in passing before,[10b] it is possible to obtain an image devoid of alignment effects by adding the three images $M_X + M_Y + M_Z$. For geometry I, M_X is the same as a 90° rotated M_Y. The summed image is proportional to the projection onto the detector plane of the zeroth-order state multipole ρ_{00}, which contains just the population distribution. However, in geometry I, the projection of ρ_{00} is independent of the in-plane angle, and all of the anisotropy information is contained in the radial distribution. This method, albeit very elegant, is therefore not a particularly sensitive measurement for a photodissociation event in which the resulting fragments are not mono-energetic. In addition, this geometry does not possess an axis of cylindrical symmetry parallel to the detector plane, so it is not possible to use the inverse Abel transform to reconstruct the distribution. In geometry II it should be possible to obtain the alignment-free image that could be reconstructed using the inverse Abel transform. However, for geometry II, the M_X image must be obtained by propagating the probe laser perpendicular to the photolysis laser. This experiment was not performed in the current study. Nevertheless, for the $O(^1D_2)$ probe, there is an interesting feature that we have exploited to get an approximation to the population-only distribution. The linestrength factors for the two lines have not been determined absolutely, but the relative values are known for the $^1F_3 \leftarrow\leftarrow {}^1D_2$ and $^1P_1 \leftarrow\leftarrow {}^1D_2$ transitions as mentioned above. These are $P_0 : P_2 : P_4 = 1 : 0.68 : 0.1$ and $1 : -0.60 : 1.1$ for the respective probe lines. As can be seen in the angular distributions obtained from the reconstructed images in Fig. 5 A and B, the two lines show contrasting behavior yielding β parameters of 0.39 and 0.64, respectively, owing to opposite contributions (arising from opposite signs of P_2) from the alignment component. By combining these two distributions weighted in such a way as to obtain the best fit to the dipole distribution, one obtains the curve shown in Fig 5 C, giving a β parameter of 0.49, in excellent agreement with values reported by Felder et al. and Houston and coworkers. In Fig. 6, we show the plot of the best-fit β parameter against the sum of square residuals χ^2 for the fit. Although this approach neglects the P_4 contribution to the distribution, it is nevertheless likely to be more accurate than fitting the results for either line uncorrected for alignment. In fact, using either probe line alone we would have obtained a value of 0.39 (for the $^1F_3 \leftarrow\leftarrow {}^1D_2$ line) or 0.64 (for the $^1P_1 \leftarrow\leftarrow {}^1D_2$ line). We will elaborate on these approaches to obtaining the anisotropy parameter with more detailed examples in a forthcoming publication.[25]

IV Discussion

Vertical electronic excitations in N_2O from the equilibrium geometry are both optically forbidden and energetically inaccessible in the vicinity of 200 nm. However, as can be

seen in the schematic potential curves of Fig. 7, based on extensive calculations of Hopper,[26] optical transitions become both allowed and energetically accessible here when the molecule is bent. This is a well-known aspect of N_2O photochemistry: Shafer et al. argued that the transition at 205.8 nm was five times more likely from the bend-excited molecule based on the temperature dependence of the absorption cross section. Hansico and Kummel studied the dependence of the $O(^1D_2)$ yield on nozzle temperature, and found a strongly increasing product yield that nearly tracked the predicted population of the bend-excited molecules in the beam. In the linear geometry, there are two singlet excited surfaces that may play a role in this process, the $A(^1\Sigma^-)$ and the $B(^1\Delta)$. The A state becomes the $1A''$ in C_s, with a minimum near 130°. The B state represents a Renner-Teller pair with the lower component, $2A'$ in C_s, also exhibiting a minimum near 130° while the second component is the $2A''$ surface, with a minimum at the linear geometry. One of the outstanding questions in N_2O photochemistry is the relative contributions of these excited states to this transition. The fact that the anisotropy parameters are positive has been taken as evidence that the $2A'$ transition dominates, and the deviation from the limiting value of 2, among other things, has sometimes been adduced as evidence that the $1A''$ state also may play a role. For the $1A''$ state, the anisotropy parameter would be -1 in the impulsive limit regardless of bending. A distinct advantage of the detailed study of orbital alignment is that it can be a probe of the excited state symmetries, allowing us to address these questions directly.

Suzuki and coworkers[7b] were the first to report orbital alignment in N_2O photodissociation, in a one-laser imaging study at 205.8 nm. This alignment was inferred from angular distributions that could not be fitted to the simple dipole distribution $I(\theta) \propto 1 + \beta P_2(\cos\theta)$. They also argued that two distinct components were present in their distributions, based principally on the fact that the observed angular distributions varied with recoil speed, and the $P(E)$ could be readily decomposed into two Gaussian components, one sharply peaked and the other quite broad. They suggested that these two components could represent either contributions of the two possible (spin-allowed) electronic transitions in this region, or nonadiabatic transitions following excitation of the dominant $A' \leftarrow A'$ transition. The β parameters were presented as a function of recoil energy, and varied from near zero for the slow products, up to nearly 1 at the peak of the translational energy distribution, then became negative for the fastest products. Neyer et al. recently reported[20] detailed measurements of the photofragment angular distributions as a function of recoil speed for dissociation near 203 nm, obtained by imaging many individual rotational levels of the N_2 product. This approach will obviously not be sensitive to the orbital alignment in the oxygen atom; in addition, they chose Q-branch transitions in N_2 so that they would not be sensitive to rotational alignment in the molecule. They found β parameters near 1 for the lower rotational levels, but decreasing sharply to near zero above J=80. They did not report an average over all the product rotational levels, so it is difficult to compare directly to the results of Suzuki et al. and to results at 193 nm. Neyer et al. used a modified impulsive model to argue qualitatively that the trend in β parameters as a function of product rotational level simply reflected increased bending in the excited state. They also indicate that there is some evidence for a contribution from the $1A'' \leftarrow 1A'$ excitation, principally based upon the alignment they observed in the $O(^1D_2)$ distributions as discussed below.

A rigorous treatment of the alignment angular distribution yields the alignment

anisotropy parameters collected in Table I. These anisotropy parameters are associated with distinct excitation mechanisms, and provide additional insights into the symmetries of the excited states, the role of nonadiabatic transitions, and the hitherto unexplored role of coherences. These anisotropy parameters can be variously expressed to yield the state multipoles, the charge cloud distribution, or the molecular frame oxygen atom density matrix. The latter includes explicitly both the magnetic sublevel distribution (represented by the diagonal elements) and the coherences (embodied in the off-diagonal elements). We show, by way of illustration, the density matrices we obtain in the molecular frame for recoil angles of 0°, 45°, and 90°, using the experimental values for the anisotropy and alignment parameters, and therefore only including the rank $K = 0, 2$ contributions:

$$\rho^{0^o}_{m'm} = \begin{pmatrix} 0.048 & 0 & 0 & 0 & 0.048 \\ 0 & 0.28 & 0 & 0.28 & 0 \\ 0 & 0 & 0.35 & 0 & 0 \\ 0 & 0.28 & 0 & 0.28 & 0 \\ 0.048 & 0 & 0 & 0 & 0.048 \end{pmatrix},$$

$$\rho^{45^o}_{m'm} = \begin{pmatrix} 0.054 & -0.0057 & 0.011 & -0.0057 & 0.054 \\ 0.0057 & 0.27 & 0.0012 & 0.27 & 0.0057 \\ 0.011 & -0.0012 & 0.35 & -0.0012 & 0.011 \\ 0.0057 & 0.27 & 0.0012 & 0.27 & 0.0057 \\ 0.054 & -0.0057 & 0.011 & -0.0057 & 0.054 \end{pmatrix},$$

$$\rho^{90^o}_{m'm} = \begin{pmatrix} 0.067 & 0 & 0.033 & 0 & 0.067 \\ 0 & 0.27 & 0 & 0.27 & 0 \\ 0.033 & 0 & 0.33 & 0 & 0.033 \\ 0 & 0.27 & 0 & 0.27 & 0 \\ 0.067 & 0 & 0.033 & 0 & 0.067 \end{pmatrix}.$$

For comparison, a statistical distribution over the magnetic sublevels would yield:

$$\rho_{m'm} = \begin{pmatrix} 0.2 & 0 & 0 & 0 & 0 \\ 0 & 0.2 & 0 & 0 & 0 \\ 0 & 0 & 0.2 & 0 & 0 \\ 0 & 0 & 0 & 0.2 & 0 \\ 0 & 0 & 0 & 0 & 0.2 \end{pmatrix}.$$

The non-zero off-diagonal elements point at the coherences that are present in this system. For comparison with earlier literature, the recoil-angle averaged magnetic

sublevel distributions are 0.34, 0.54 and 0.12, for the $|m| = 0$, 1, and 2 sublevels, respectively. This indicates that **J** is pointing predominantly perpendicular to the recoil direction; in the vector model,[27] the cone on which **J** is precessing would make a ~70° angle with the recoil axis. Our sublevel populations compare to values reported by Chandler et al.[19] of 0.37, 0.63, and 0, respectively for the oxygen atom co-fragment to the N_2 (J=66) product, and 0.53, 0.12, and 0.35, respectively, for that corresponding to N_2 (J=82). They used a treatment that assumes the m-populations are all independent and neglects all coherences.

The alignment distributions are dominated by a strong s_2 and somewhat weaker α_2 contribution, implying incoherent parallel and perpendicular components to the excitation. This may well reflect the different components of the $2A' \leftarrow 1A'$ excitation in the recoil frame. It is important to note that both singlet transitions are strictly forbidden for the linear molecule. The orientation of the transition moment is thus an important, nontrivial question, even for the $2A' \leftarrow 1A'$ excitation. The assumption that the transition moment is aligned along the N–O bond direction is clearly invalid for this transition. Qualitative estimates suggest that the transition moment is directed at large angles from the N–O bond axis for N–N–O angles near linear, and it is only when the molecule is sharply bent that the transition moment begins to align with the N–O bond. Examination of the potential curves of Hopper can provide a rough estimate of the degree of bending necessary to make the transition energetically allowed. For fixed bond distances, excitation to the $2A'$ surface at 193 nm becomes possible for bond angles 20° or so from linear as indicated in Fig. 8. This value is likely to be reduced by bond stretching, which is also expected to play a role. The value of 0.5 for β corresponds, in the prompt limit for a single transition, to recoil at an angle of 45° from the transition moment. Although it is possible to achieve this angle for the $2A' \leftarrow 1A'$ transition, by invoking excitation from near-linear geometries at which the transition moment may be up to 45° from the N–O bond, there is clear evidence in the coherences that the $1A'' \leftarrow 1A'$ also plays a role. The impact of a contribution from this transition will be to reduce the effective β value.

The large s_2 value is a manifestation of the predominant incoherent, intrinsic vector correlation that vanishes after averaging over recoil angles. Comparison of the s_2 and α_2 values gives the ratio of the parallel and perpendicular alignment dynamical functions[10b,13] $f_2(0,0) / f_2(1,1) \approx 2.2$. This implies that most of the alignment is produced via the parallel transition, consistent with the overall positive β parameter. We can transform these results to the molecular frame using Eq. (17) of Ref. 10b. We find the molecular-frame diagonal alignment parameter $\langle A_{20}^{mol} \rangle$ is always negative, implying that the corresponding angular momentum vector **J**, for any recoil direction, is mainly perpendicular to the recoil axis.

In addition to the dominant incoherent contributions to the orbital alignment, a perpendicular coherence is clearly observed, implied by the nonzero η_2 value. This can be accounted for in several ways: (a) coherent excitation of the perpendicular components of the $2A' \leftarrow 1A'$ transition, (b) coherent excitation of the pure perpendicular $1A'' \leftarrow 1A'$ transition, or (c) through simultaneous, coherent excitation of the perpendicular component of the $2A' \leftarrow 1A'$ transition and the pure perpendicular $1A'' \leftarrow 1A'$ transition. The destiny of either one of these coherent superpositions depends on the details of the following dynamics leading to the observed value of the η_2 alignment parameter, which

will require further theoretical study. The η_2 parameter is related to the $\langle A_{20}^{mol} \rangle$ molecular frame alignment component,[10b] and ranges from 0 for recoil along the direction of the transition moment, to $\approx -\sqrt{6/10}$ at $\theta = \pi/2$, about 2/5 of its minimum possible value. The corresponding angular momentum **J** is again perpendicular to the recoil axis.

Future theoretical studies will be required for a quantitative analysis of the results, including the detailed implications for the relative contributions of the two electronic transitions and the role of non-adiabatic transitions in the dissociation process. This work is underway.

V Conclusion

We have observed strong recoil-frame orbital alignment in the $O(^1D_2)$ product following photodissociation of N_2O at 193.3 nm using velocity map imaging. The method allows for investigation of the angular distribution of this alignment, providing insight into the dynamics in the frame of the molecule. We have analyzed the results using a rigorous quantum mechanical theory to obtain alignment anisotropy parameters having direct physical significance. The results provide detailed insight into the dynamics of the photodissociation process and the nature of the electronic transitions responsible for the initial excitation. The alignment is dominated by strong incoherent parallel and perpendicular contributions which reflect mainly the two components of the $2A' \leftarrow 1A'$ transition. In addition, we find evidence of a contribution from a coherence between two perpendicular transitions. The latter observation may hint at the direct evidence for a contribution of the $1A'' \leftarrow 1A'$ transition to N_2O photoexcitation in the ultraviolet, subject to more detailed theoretical scrutiny.

The authors acknowledge Dr. D. W. Chandler for providing preprints of their N_2O work, and Dr. A. S. Bracker for helpful discussions. This work was supported by the Director, Office of Science, Office of Basic Energy Sciences, Chemical Sciences Division of the U.S. Department of Energy under contract No. DEACO3–76SF00098.

References

1. J. P. Simons, *J. Phys. Chem.*, 1987, **91**, 5378.
2. *(a)* R. N. Zare and D. R. Herschbach, *Proc. IEEE,* 1963, **51**, 173; *(b)* J. H. Ling and K. R. Wilson, *J. Chem. Phys.*, 1976, **65**, 881; *(c)* C. H. Green and R. N. Zare, *Annu. Rev. Phys. Chem.*, 1982, **33**, 119; *(d)* R. B. Bernstein, D. R. Herschbach and R. D. Levine, *J. Phys. Chem.*, 1987, **91**, 5365; G. E. Hall, N. Sivakumar, D. Chawala and P. L. Houston, *J. Chem. Phys.*, 1988, **88**, 3682; *(g)* M. N. R. Ashfold, I. R. Lambert, D. H. Mordaunt, G. P. Morley and C. M. Western, *J. Phys. Chem.*, 1982, **96**, 2938; *(h)* S. W. North and G. E. Hall, *J. Phys. Chem.*, 1996, **104**, 1864.
3. *(a)* G. E. Busch, R. T. Mononey, R. I. Morse and K. R. Wilson, *J. Chem. Phys.*, 1969, **51**, 837; *(b)* R. N. Zare, *Mol. Photochem.*, 1972, **4**, 1; *(c)* G. E. Busch and K. R. Wilson, *J. Chem. Phys.*, 1972, **56**, 3626.
4. *(a)* R. J. Van Brunt and R. N. Zare, *J. Chem. Phys.*, 1968, **48**, 4304; *(b)* E. W. Rothe, U. Krause and R. Düren, *Chem. Phys. Lett.*, 1980, **72**, 100; *(c)* O. S. Vasyutinskii, *JETP Lett.*, 1980, **31**, 428; *Sov. Phys. JETP*, 1981, **54**, 855; *(d)* J. Vigué, P. Grangier, A. J. Aspect, *J. Phys. Lett. (Paris)* 1981, **42**, L531; *(e)* J. Vigué, J. A. Beswick and M. J. Broyer, *J. Phys. (Paris)* 1983, **44**, 1225; *(f)* H. Kato and K. J. Onomichi, *J. Chem. Phys.*, 1985, **82**, 1642; *(g)* H. Kato, *Faraday Discuss. Chem. Soc.*, 1986, **82**, 1; *(h)* V. Zafiropulos, P. D. Kleiber, K. M. Sando, X. Zeng, A. M. Lyyra and W. C. Stwalley, 1988, **61**, 1485; *(i)* P. D. Kleiber, J.-X. Wang, K. M. Sando, V. Zafiropulos and W. C. Stwalley, *J. Chem. Phys.*, 1991, **95**, 4168.
5. K. Blum, *Density Matrix Theory and Applications, 2nd Ed.*, Plenum, New York, 1996.
6. *(a)* R. N. Dixon, *J. Chem. Phys.* 1986, **85**, 1866; *(b)* G. E. Hall, Sivakumar, P. L. Houston and I. Burak, *Phys. Rev. Lett.*, 1986, **56**, 1671; *(c)* P. L. Houston, *J. Phys. Chem.*, 1987, **91**, 5388; *(d)* R. J. Gordon and G. E. Hall, *Adv. Chem. Phys.*, 1996, **96**, 1.
7. *(a)* Y. Mo, H. Katayanagi, M. C. Heaven and T. Suzuki, *Phys. Rev. Lett.*, 1996, **77**, 830; *(b)* T. Suzuki, H. Katayanagi, Y. Mo and K. Tonokura, *Chem. Phys. Lett.*, 1996, **256**, 90; *(c)* A. T. J. B. Eppink, D. H. Parker, M. H. M. Janssen, B. Buijsse and W. J. van der Zande, *J. Chem. Phys.*, 1998, **108**, 1305.
8. Y. Wang, H. P. Loock, J. Cao and C. X. W. Qian, *J. Chem. Phys.*, 1995, **102**, 808.
9. T. P. Raktizis, S. A. Kandel, and R. N. Zare, *J. Chem. Phys.* 1998, **108**, 8291.
10. *(a)* A. S. Bracker, E. R. Wouters, A. G. Suits, Y. T. Lee and O. S. Vasyutinskii, *Phys. Rev. Lett.*, 1997, **80**, 1626; *(b)* A.S. Bracker, E. R. Wouters, O. S. Vasyutinskii and A.G. Suits, *J. Chem. Phys.* (in press); *(c)* M. Ahmed, D. S. Peterka, A. S. Bracker, O. S. Vasyutinskii and A. G. Suits, *J. Chem. Phys.,* 1999, **110**, 4115.
11. *(a)* T. P. Rakitzis, S. A. Kandel, A. J. Alexander, Z. H. Kim and R. N. Zare, *J. Chem. Phys.* 1998, **110**, 3341; *(b)* T. P. Rakitzis, S. A. Kandel, A. J. Alexander, Z. H. Kim and R. N. Zare, *J. Chem. Phys.* 1998, **110**, 3351.
12. L. D. A. Siebbeles, M. Glass-Maujean, O. S. Vasyutinskii, J. A. Beswick and O. Roncero, *J. Chem. Phys.*, 1994, **100**, 3610.
13. B. V. Picheyev, A. G. Smolin and O. S. Vasyutinskii, *J. Phys. Chem.*, 1997, **101,** 7614.
14. *(a)* A. J. Alexander, F. J. Aoiz, M. Brouard, J. P. Simons, *Chem. Phys. Lett.* 1996, **256,** 561; *(b)* A. J. Alexander, F. J. Aoiz, L. Bañares, M. Brouard, I. Burak, Y. Fujimura, J. Short, J. P. Simons, *Chem. Phys. Lett.* 1996, **262,** 589; *(c)* A. J. Alexander, F. J. Aoiz, L. Bañares, M. Brouard, J. Short, J. P. Simons, *J. Phys. Chem. A*, 1997, **101**, 7544.
15. P. Felder, B. M. Haas and J. R. Huber, *Chem. Phys. Lett.*, 1991, **186**, 177.
16. L. L. Springsteen, S. Satyapal, Y. Matsumi, L. M. Dobeck and P. L. Houston, *J. Phys. Chem.*, 1993, **97**, 7239.
17. N. Shafer, K. Tonokura, Y. Matsumi, S. Tasaki, and M. Kawasaki, *J. Chem. Phys.* 1991, **95**, 6218.

18. T. F. Hansico and A. C. Kummel, *J. Phys. Chem.*, 1993, **97**, 7242.
19. M. H. M. Janssen, J. M. Teule, D. W. Neyer, D. W. Chandler and S. Stolte, *Faraday Disc.*, 1997, **108**, 435.
20. D. W. Neyer, A. J. R. Heck and D. W. Chandler, *J. Chem. Phys.*, 1999, **110**, 3411.
21. M. Ahmed, D. A. Blunt, D. Chen, and A.G. Suits, *J. Chem. Phys.*, 1997, **106**, 7617.
22. S. Pratt, P. M. Dehmer and J. L. Dehmer, *Phys. Rev. A*, 1991, **43**, 4702.
23. A. T. J. B. Eppink and D. H. Parker, *Rev. Sci. Instrum.*, 1997, **68**, 3477.
24. Y. Mo and T. Suzuki, *J. Chem. Phys.*,1998, **109**, 4691.
25. E. R. Wouters, M. Ahmed, D. S. Peterka, O. S. Vasyutinskii and A. G. Suits, in preparation.
26. D. G. Hopper, *J. Chem. Phys.*,1984, **80**, 4290.
27. R. N. Zare, *Angular Momentum*, World Scientific, New York, 1988.

Tables

TABLE I. Alignment parameters obtained from the two approaches to fit the difference images. The digits in parentheses are the one-standard deviation uncertainty in the last digit of the given value.

Alignment parameter	SVD fit	Ring fit	Interpretation
s_2	–0.082(13)	–0.097(27)	incoherent parallel and perpendicular
α_2	0.022(14)	0.031(18)	incoherent parallel and perpendicular
η_2	0.017(5)	0.039(10)	coherent perpendicular
γ_2	–0.003(10)	–0.016(20)	coherent parallel and perpendicular

Figure Captions

FIG. 1. Schematic view of the experimental setup.

FIG. 2. Data images for $O(^1D_2)$ from photodissociation of N_2O at 193.3 nm. Upper panel, experimental data for indicated combinations of photolysis and probe laser polarizations. Lower panel, difference images obtained from data and the SVD fit, representing alignment angular distributions. The background in the difference images is zero (white); difference signal is positive (blue) or negative (red).

FIG. 3. Total translational energy distribution for $O(^1D_2)$ from the image in the second row, second column (both laser polarizations in the detector plane) of Fig. 2.

FIG. 4. Fits to the alignment (difference) images of Fig. 2 obtained by analysis of the angular behavior of the outer portion of the distribution (A) geometry I; (B) geometry II.

FIG. 5. Angular distributions obtained from inverse Abel transform of images obtained using (A) ($^1P_1 \leftarrow\leftarrow {}^1D_2$) probe transition at 205.8 nm; (B) ($^1F_3 \leftarrow\leftarrow {}^1D_2$) probe transition at 203.5 nm and (C) linear combination of (A) and (B) curves yielding best-fit to dipole distribution (see Fig. 7).

FIG. 6. Error in fit to dipole distribution (χ^2) as a function of anisotropy parameter β for linear combinations of curves in Fig. 6 A and B.

FIG. 7. Schematic potential curves for N_2O adapted from Ref. 25. A) Dependence on N–O bond distance, showing curve crossing region (for 130° N–N–O angle). b) Dependence on bending angle for fixed bond distances: N–N 1.1 Å; N–O 1.4Å. The arrow indicates the angle for which 193 nm excitation is energetically allowed.

FIG 1

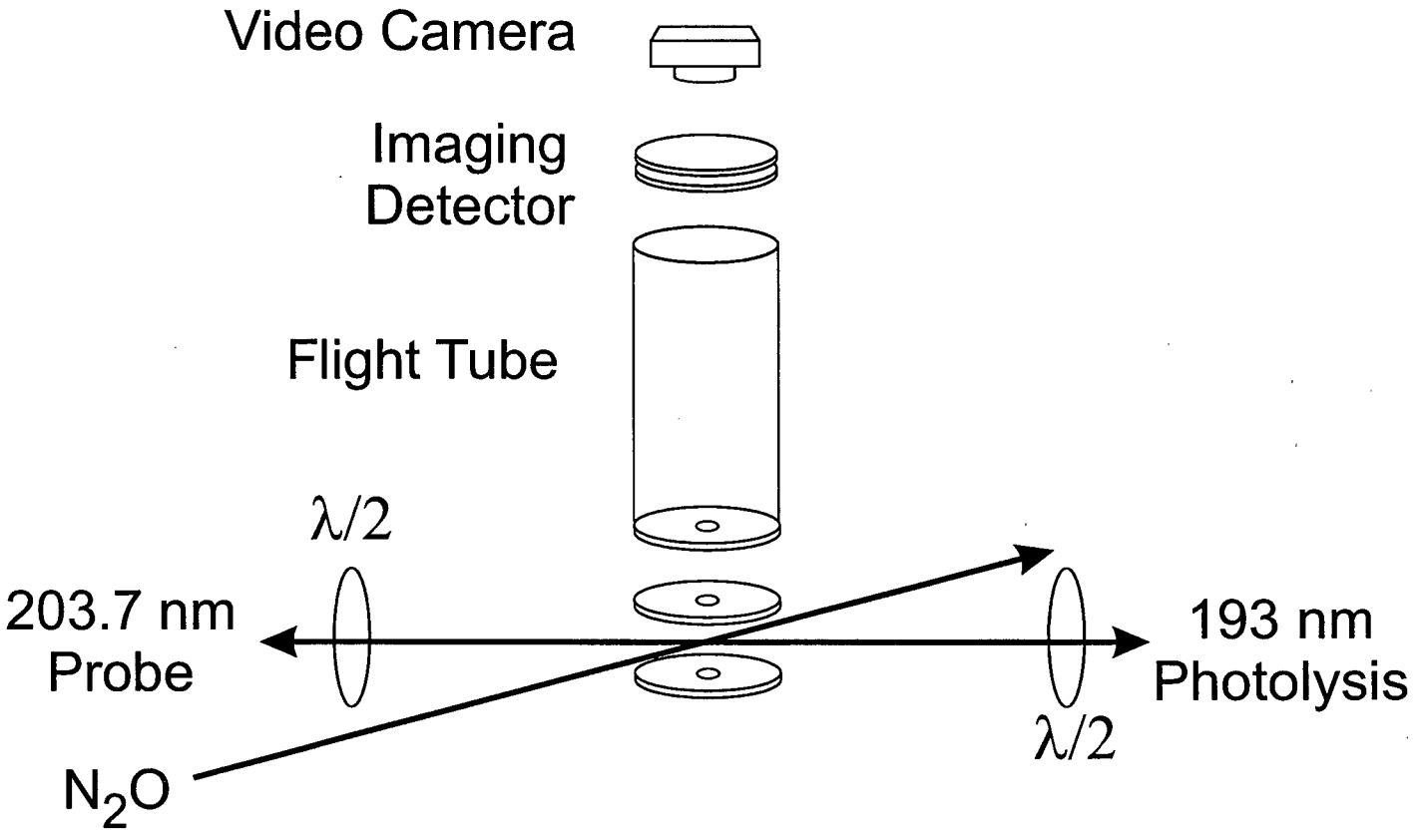
Video Camera
Imaging Detector
Flight Tube
λ/2
203.7 nm Probe
193 nm Photolysis
λ/2
N_2O

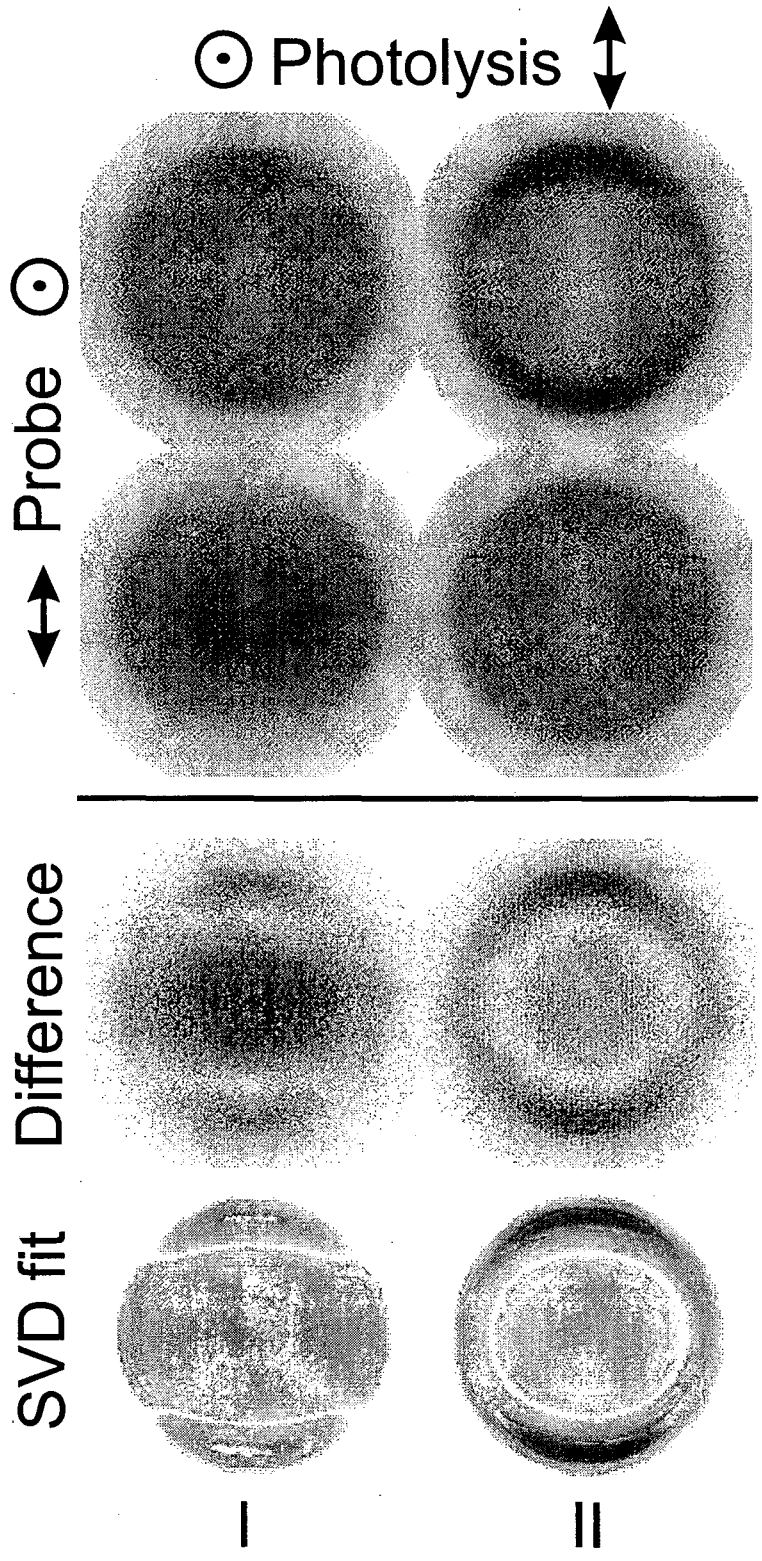

Fig. 2

FIG. 3

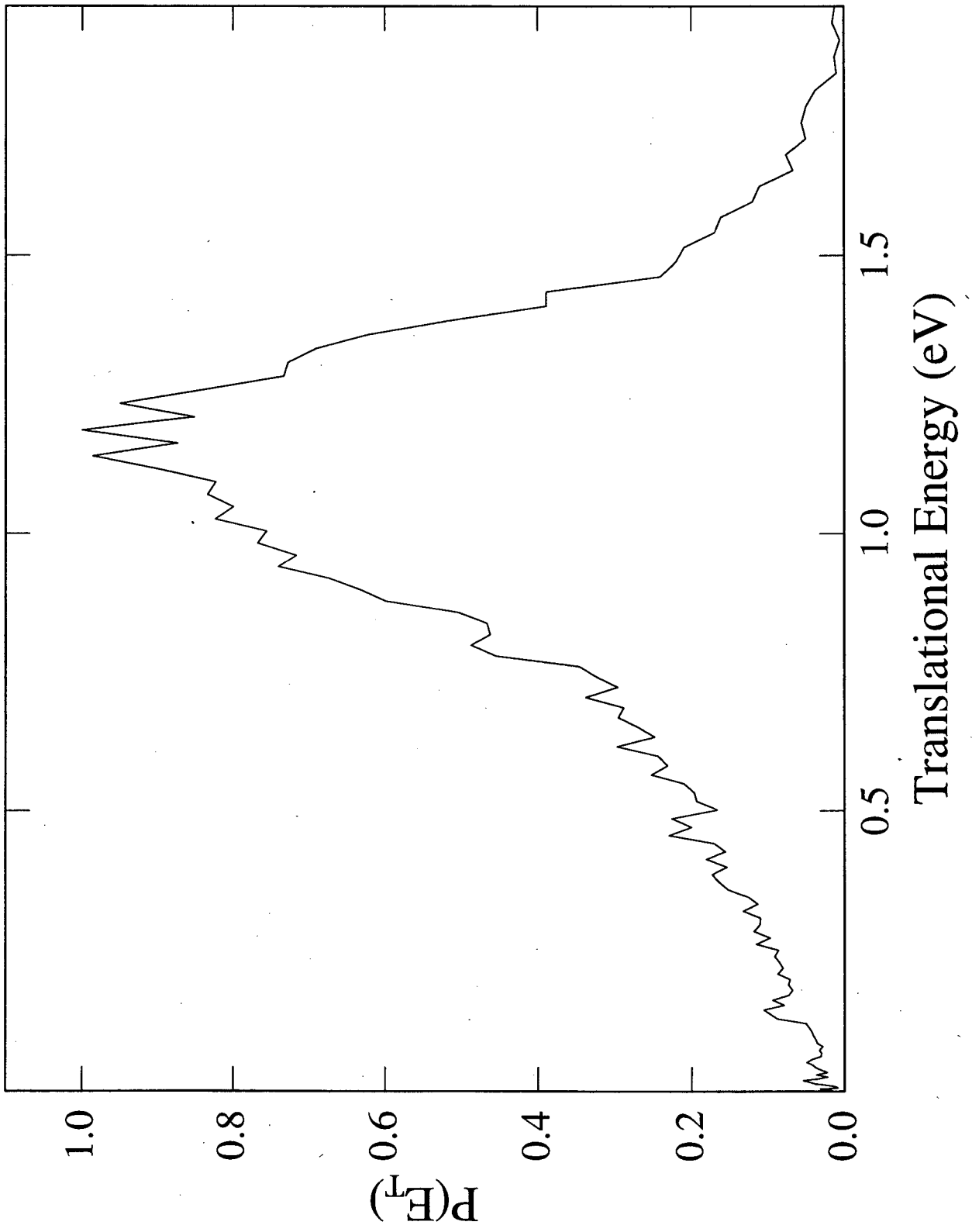

FIG. 4

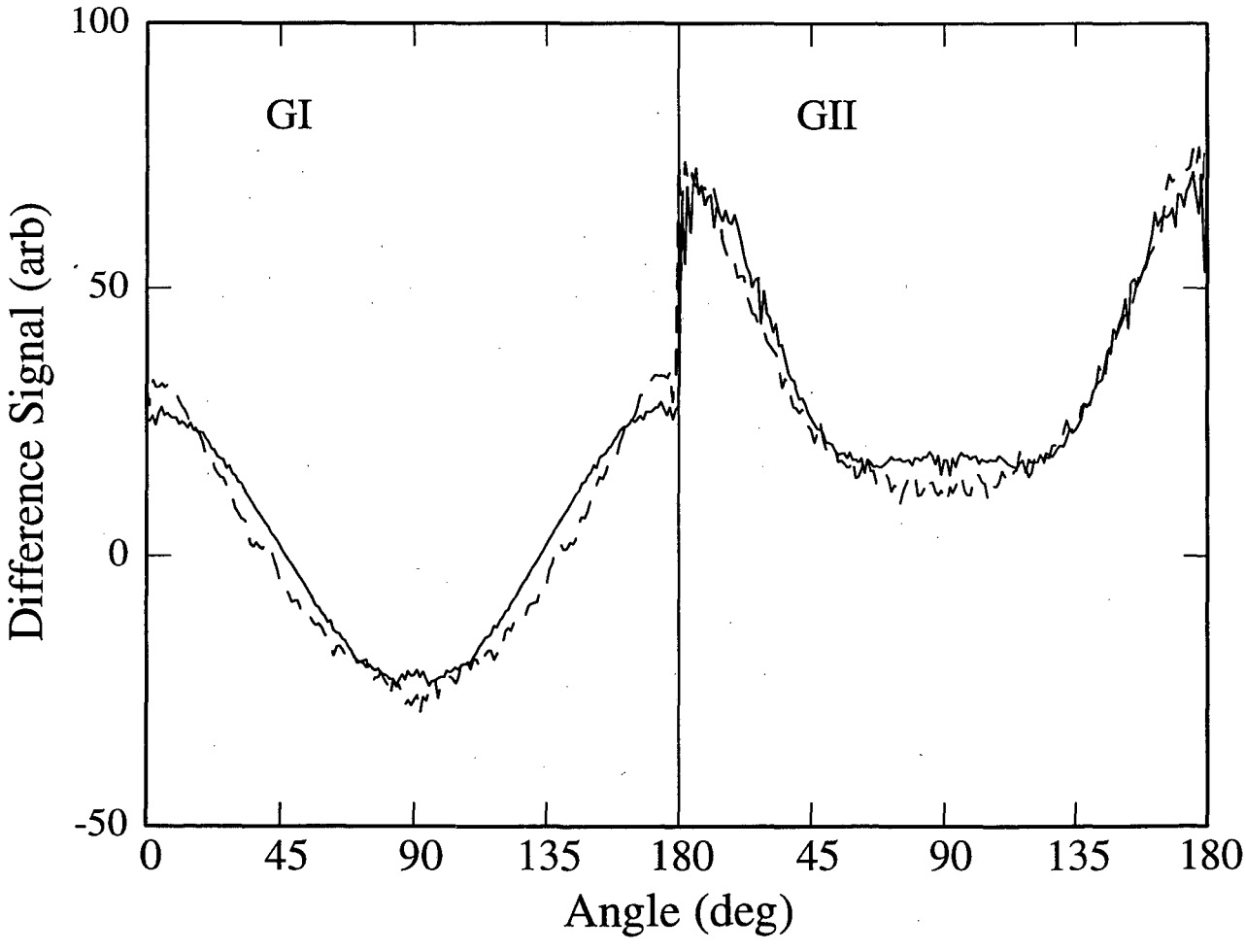
100
50
0
-50
GI
GII
Difference Signal (arb)
0
45
90
135
180
45
90
135
180
Angle (deg)

FIG. 5

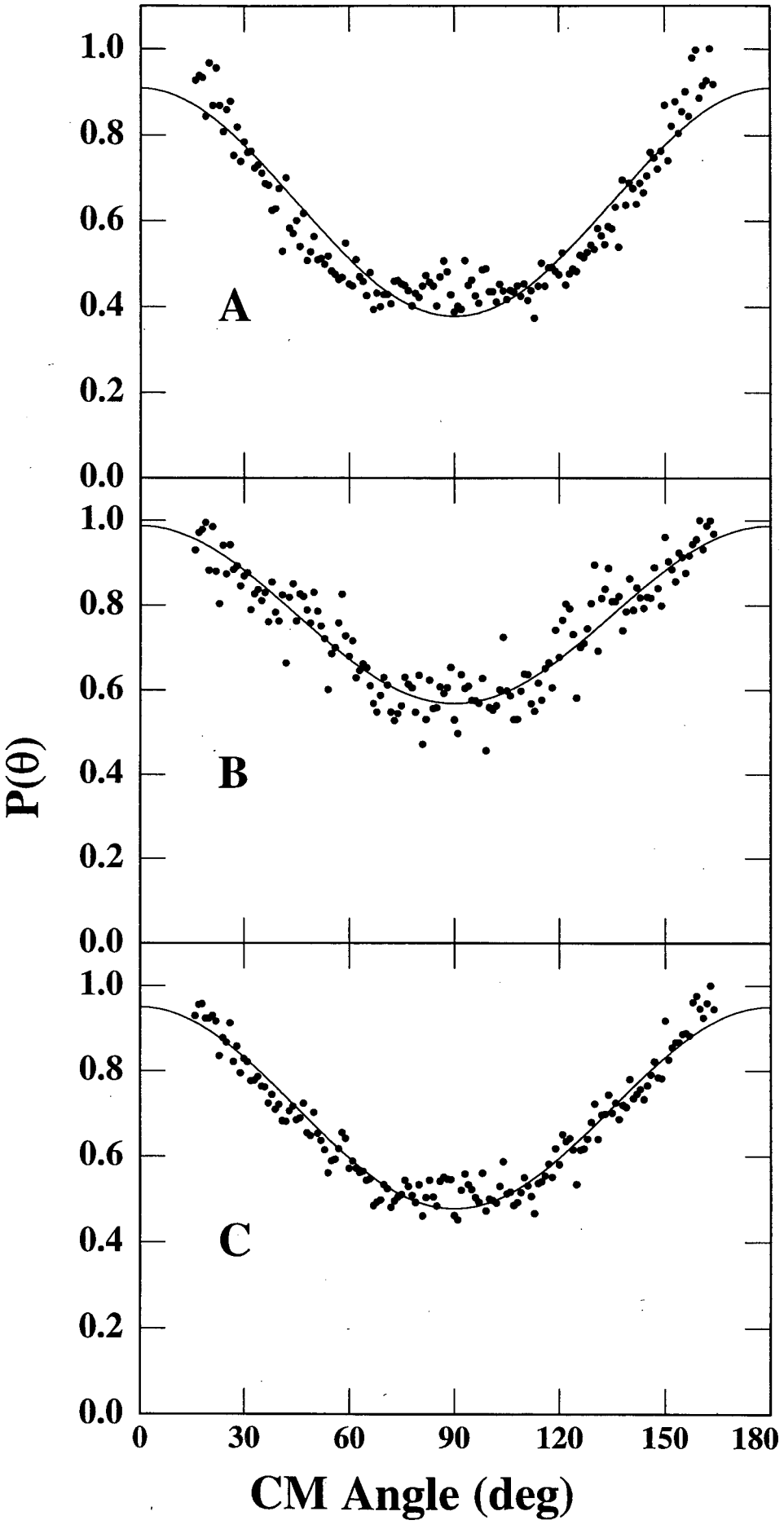

FIG. 6

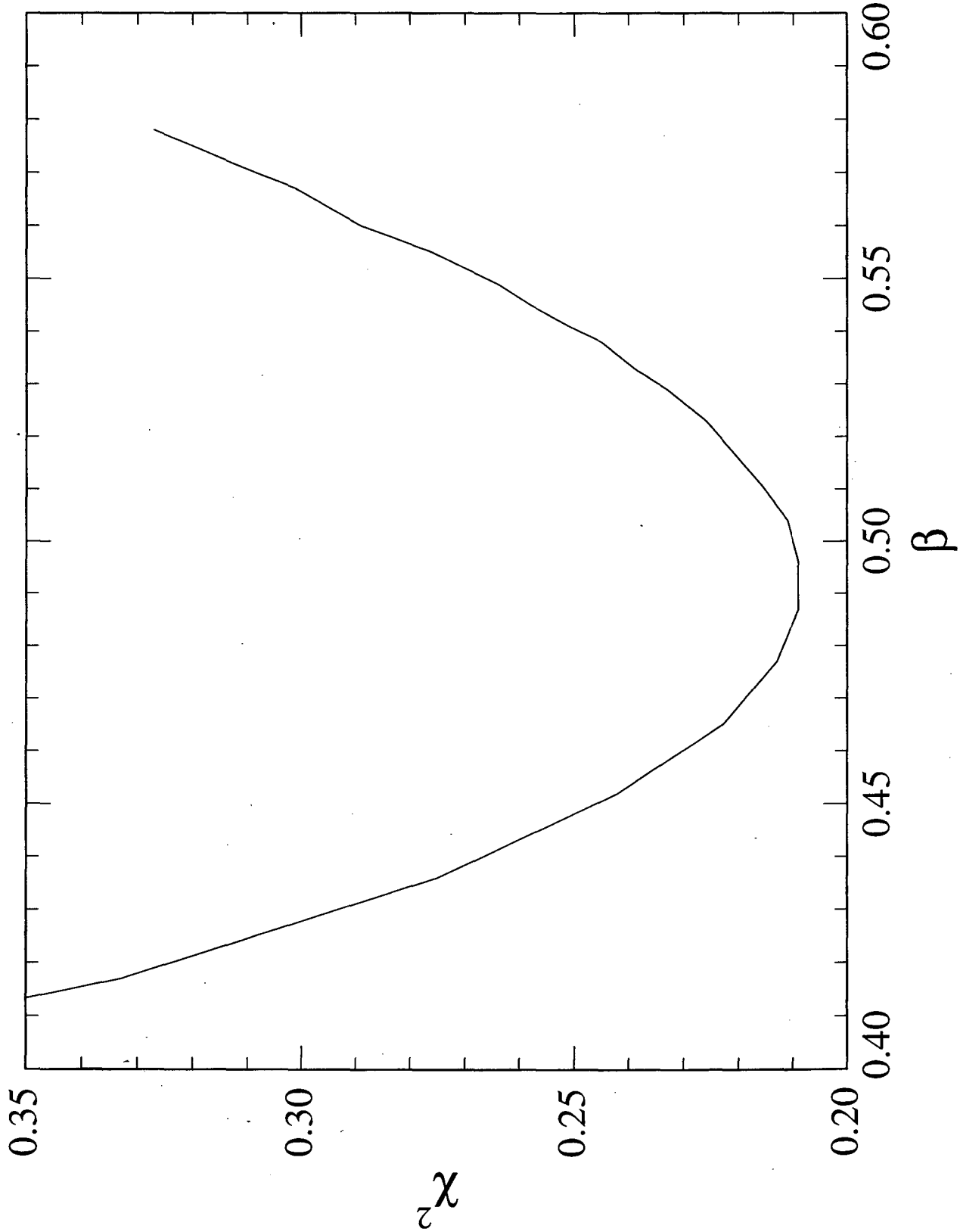

FIG. 7

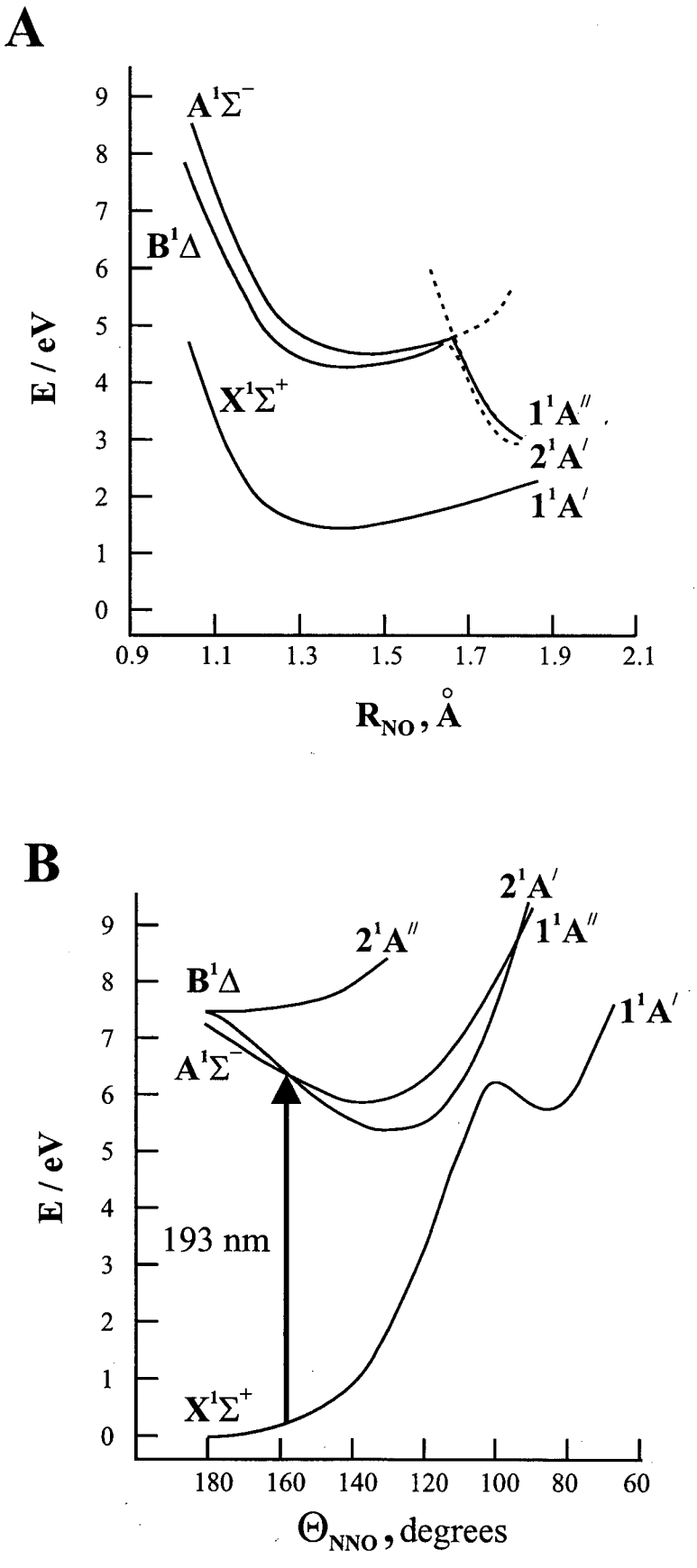
A
E / eV
$A^1\Sigma^-$
$B^1\Delta$
$X^1\Sigma^+$
$1^1A''$
$2^1A'$
$1^1A'$
R_{NO}, Å
B
$2^1A'$
$1^1A''$
$2^1A''$
$B^1\Delta$
$1^1A'$
$A^1\Sigma^-$
193 nm
$X^1\Sigma^+$
Θ_{NNO}, degrees

Ernest Orlando Lawrence Berkeley National Laboratory
One Cyclotron Road Berkeley, California 94720

Prepared for the U.S. Department of Energy under Contract No. DE-AC03-76SF00098